

Estimating external magnetic field differences at high geomagnetic latitudes from a single station

Ciarán D. Beggan*, Laurence Billingham and Ellen Clarke†

Geomagnetism, British Geological Survey, Riccarton, Edinburgh, EH14 4AP, UK

Received July 2017, revision accepted February 2018

ABSTRACT

Providing an accurate estimate of the magnetic field on the Earth's surface at a location distant from an observatory has useful scientific and commercial applications, such as in repeat station data reduction, space weather nowcasting or aeromagnetic surveying. While the correlation of measurements between nearby magnetic observatories at low and mid-latitudes is good, at high geomagnetic latitudes ($58\text{--}75^\circ$) the external field differences between observatories increase rapidly with distance, even during relatively low magnetic activity. Thus, it is of interest to describe how the differences (or errors) in external magnetic field extrapolation from a single observatory grow with distance from its location. These differences are modulated by local time, seasonal and solar cycle variations, as well as geomagnetic activity, giving a complex temporal and spatial relationship. A straightforward way to describe the differences are via confidence intervals for the extrapolated values with respect to distance. To compute the confidence intervals associated with extrapolation of the external field at varying distances from an observatory, we used 695 station-years of overlapping minute-mean data from 37 observatories and variometers at high latitudes from which we removed the main and crustal fields to isolate unmodelled signals. From this data set, the pairwise differences were analysed to quantify the variation during a range of time epochs and separation distances. We estimate the 68.3%, 95.4% and 99.7% confidence levels (equivalent to the 1σ , 2σ and 3σ Gaussian error bounds) from these differences for all components. We find that there is always a small non-zero bias that we ascribe to instrumentation and local crustal field induction effects. The computed confidence intervals are typically twice as large in the north–south direction compared to the east–west direction and smaller during the solstice months compared to the equinoxes.

Key words: Data processing, Extrapolation, Magnetics, Modelling.

1 INTRODUCTION

Any measurement of the geomagnetic field on or near the Earth's surface is composed of contributions from a number of sources including the main field, crustal field and various external fields. Typically, over 95% of the total field strength comes from the core with the remainder supplied by the lithospheric and external fields (e.g.

Campbell 2003). The magnetic field also varies over a spectrum of time-scales from micro-seconds to millions of years (e.g. Constable 2015), with each contribution distinguished by both its source location and temporal signature. Some sources such as the slowly varying main field (Olsen *et al.* 2015) and the large-scale (>300 km) crustal field (e.g. Thébault *et al.* 2010) are relatively easy to measure and model, and dedicated satellite missions such as Swarm and CHAMP allow high-fidelity models to be constructed that characterize the spatial and temporal behaviour of these fields extremely well.

*E-mail: ciar@bgs.ac.uk

†Equally contributing authors.

External field sources, however, can be large, dynamic and difficult to predict even within well-understood systems such as the diurnal Solar quiet (Sq) current (Sabaka *et al.* 2015). During geomagnetic storms at high latitudes, external field variation can rise to over 8% (e.g. >4000 nT) of the total field strength particularly when both ionospheric and magnetospheric current systems become highly active (e.g. Gjerloev and Hoffman 2014). Even at globally geomagnetically quiet times we can expect features like Flux Transfer Events (i.e. patchy dayside reconnection) to give ~100 nT perturbations on ground scales of 100 km (McHenry and Clauer 1987), or substorms that have coherent excursions of >500 nT extending from 5 to 10 degrees in latitude (Ritter and Lühr 2008). As a detailed understanding of the linkage between solar and geomagnetic activity remains an open area of research (Juusola *et al.* 2015), there are still no reliable methods of modelling or forecasting the localized external fields generated during geomagnetic storms.

Accurately estimating the full field magnetic vector across the Earth has many useful scientific and practical applications, for example in reduction to quiet-time values in repeat station surveying, space weather nowcasting (Gaunt 2016), aeromagnetic surveying (Reeves 1993) or commercial activities such as directional drilling (Reay *et al.* 2005; Edvardsen, Johnsen and Lovhaug 2016). In many of these scenarios, the location of interest is typically remote from a geomagnetic observatory or variometer. Though the internal magnetic fields can be computed from main and crustal field models, the external field values must first be measured and extrapolated to the time and position of interest.

If data from more than one station are available, a number of techniques have been developed to extrapolate the external magnetic field across large regions. The most basic method is a simple mathematical interpolation between two observatories, taking into account the weighted latitude difference (e.g. Reay *et al.* 2005). A physics-based approach called Spherical Elementary Current Systems (Amm and Viljanen 1999) is useful when a number of observatories are available surrounding the site of interest. This method produces a better recovery of the magnetic field than latitudinal weighted extrapolation under suitable spatial configurations of the observatory or variometer stations (McLay and Beggan 2010). Waters *et al.* (2015) have suggested a statistical-based method using Principal Component Analysis for infilling regions where magnetic data are lacking, while Dods, Chapman and Gjerloev (2015) have shown topological linkages between observatories within a network analysis framework, showing strong correlations exist between data

at different latitudes during similar phases of geomagnetic storms.

However, due to the general paucity of ground-based magnetic instruments across the globe, in many areas measurements for estimating the external field in real-time or for off-line post-processing are often only available from a single observatory or variometer. In these cases, the errors in the external field values given to the user at their location are directly dependent on distance from the station, geomagnetic latitude and geomagnetic activity. Even though this is the worst-case scenario, it occurs commonly. An analytical solution for some of the errors involved in creating main and crustal models can be computed from the known limitations of the methodology (e.g. Finlay *et al.* 2010), but most error studies rely on comparisons with observatory data and spot or repeat station measurements, if available, to estimate the difference between the models and the true field values at the surface.

As well as an estimate for the magnetic field at a particular time and location from a single measurement site, an associated value for the error is relevant for many applications, for example to identify outliers when using data in inverse models, quality control during directional drilling or to control tie-points along flight lines. The error of the extrapolated value from one location to another can be parameterized using three basic properties: distance, geomagnetic latitude and epoch (e.g. by season or solar cycle phase). An analysis of the typical size of such errors can thus be made by examining the differences between proximal and distal observatory and variometer data over long periods of time (i.e. years to decades). Several other studies have looked at similar statistics, but for relatively short time periods (Watermann *et al.* 2006) or at lower geomagnetic latitudes (Gleisner, Rasmussen and Watermann 2006).

For this study, we adopt the same approach and examine over 3000 years of minute-mean vector data from 37 observatories and variometers at high geomagnetic latitudes, covering the digital magnetometer era (from the late 1970s). The aim is to develop an understanding of the differences in the external field between measurements at multiple locations over long periods of time and compute the associated confidence limits. This will enable us to determine the maximum distance that external field values from a measurement site can be reliably used, given the three parameters of geomagnetic latitude, distance and direction (north–south or east–west), and epoch. This analysis implicitly captures data at all magnetic activity levels and so gives a conservative, or more general, baseline for the errors.

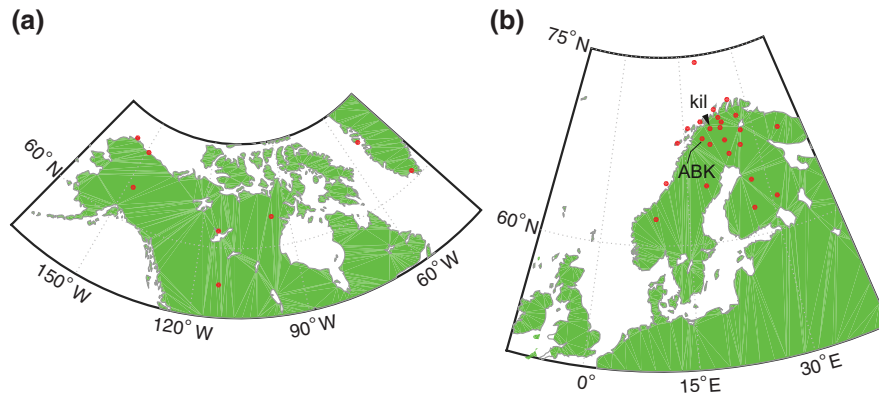


Figure 1 Locations of (a) the 10 stations in North America and (b) the 25 stations (closed circles) in Scandinavia used in this study. The positions of the Abisko observatory (ABK) and Kilpisjärvi variometer (kil) are shown.

In Section 2, we describe the observatory and variometer data and methodology used to separate the external field. Section 3 examines the results with a general example from a station-pair in Scandinavia separated by 110 km and a special case of two closely located observatories in Alaska, before showing the overall results. We discuss our findings in further detail in Section 4.

2 DATA AND METHODOLOGY

2.1 Data selection

We obtained observatory data from World Data Centre (WDC) for Geomagnetism (Edinburgh) using its RESTful web service (Dawson *et al.* 2013) and filtered the data by the following criteria: station geomagnetic latitude, pairwise distances between stations and availability of overlapping time series. We focused on high geomagnetic latitudes where the external field contribution is most significant, restricting the study to a set of stations at geomagnetic latitudes between 58° and 75° (north or south), with latitude defined in quasi-dipole coordinates (Emmert, Richmond and Drob 2010) evaluated for the 2014.0 epoch. We then applied three further constraints based on consideration of the pairs of stations together: (1) the great circle distance between the stations must be less than 1000 km, (2) each member of the pair must have minute-mean data available (as compared to hourly means) and (3) there must be at least one year of data in common between the pair.

After applying these constraints, relatively few WDC observatories remained. We thus acquired further data from the International Monitor for Auroral Geomagnetic Effects (IMAGE) network in northern Scandinavia (Tanskanen

2009). These observatory and variometer data were subject to the same selection criteria as the data from the WDC, including cross IMAGE-WDC pairs. Figure 1(a) shows a map of the WDC observatory locations used in North America and Greenland and Fig. 1(b) shows a map of the IMAGE and WDC station locations used in the most heavily populated region of northern Scandinavia. We highlight two stations, the observatory Abisko (ABK) run by the Geological Survey of Sweden and variometer Kilpisjärvi (kil) operated by Sodankylä Geophysical Observatory; both are used as examples later in the paper.

After further visual inspection of the individual data sets, those which showed copious and obvious spikes or steps throughout the time series were rejected. The final studied data set consists of 37 stations that give 695 paired-years of minute-mean data. Although visibly poor data were eliminated, the volume of data involved makes detailed quality control of every datum impractical. Hence, it is likely that some erroneous data remain in the set under study, given the trade-off made between overall data quality and coverage. There are 267 pairs of stations that meet all our criteria in the final data set and the total volume of overlapping data is equivalent to around 3000 years. Whilst the shortest overlapping period is one year, the longest is more than two solar cycles. Table 1 gives the list of station codes, location and number of years of data selected from each location. Note that there is only a single station-pair in the Southern hemisphere.

2.2 Baseline removal

In order to compute the uncertainties in extrapolating magnetometer data to distance, we attempt to mimic the processes used when applying external field estimates in real-time. To

Table 1 Table of station code, name, location and Quasi-Dipole (QD) geomagnetic coordinates^a and number of years available. Stations with capitalised codes are observatories, while lower case codes are variometers in the IMAGE network

Code	Name	Latitude°	Longitude°	QD Latitude°	QD Longitude°	Years
ABK	Abisko	68.35	18.82	65.5	100.6	31
alt	Alta	69.86	22.96	66.9	105.1	9
and	Andenes	69.30	16.03	66.6	99.1	14
bjn	Bear Island	74.50	19.20	71.7	106.4	25
BLC	Baker Lake	64.32	263.99	73.1	330.7	31
BRW	Barrow	71.30	203.38	70.4	254.6	35
CMO	College	64.87	212.14	65.2	266.9	35
DED	Deadhorse	70.36	211.21	70.6	261.8	2
DOB	Dombås	62.07	9.11	59.3	89.3	12
DVS	Davis	-68.58	77.97	-74.8	101.8	9
FCC	Fort Churchill	58.76	265.91	68.0	334.9	30
GDH	Qeqertarsuaq	69.25	306.46	74.8	38.0	29
han	Hankasalmi	62.25	26.60	58.9	104.0	19
hop	Hopen Island	76.51	25.01	73.4	113.5	18
HRN	Hornsund	77.00	15.55	74.4	107.5	19
IQA	Iqaluit	63.75	291.48	71.6	15.1	15
iva	Ivalo	68.56	27.29	65.4	107.6	10
JCO	Jim Carrigan	70.36	211.20	70.6	261.8	2
kau	Kautokeino	69.02	23.05	66.0	104.5	8
kil	Kilpisjärvi	69.06	20.7	66.1	102.7	28
KIR	Kiruna	67.84	20.42	64.9	101.6	17
lek	Leknes	68.13	13.54	66.5	96.1	5
loz	Lovozero	67.97	35.08	64.6	113.8	14
LYC	Lycksele	64.61	18.75	61.6	98.4	13
mas	Masi	69.46	23.70	66.4	105.3	20
MAW	Mawson	-67.60	62.88	-70.4	91.8	9
MEA	Meanook	54.62	246.65	61.6	68.3	28
mek	Mekrijärvi	62.77	30.97	59.4	108.0	7
NAQ	Narsarsuaq	61.17	314.57	65.2	42.5	25
ouj	Oulujärvi	64.52	27.23	61.2	105.5	19
pel	Pello	66.90	24.08	63.8	104.1	28
rvk	Rørvik	64.94	10.98	62.3	92.3	12
SOD	Sodankylä	67.37	26.63	64.2	106.4	30
sol	Solund	61.08	4.84	58.4	85.4	5
sor	Sørøya	70.54	22.22	67.6	105.0	24
TRO	Tromsø	69.66	18.94	66.9	101.7	28
YKC	Yellowknife	62.48	245.52	69.1	304.0	28

^a at 2014.0

begin with we use the full vector field as reported by each observatory (or variometer) and perform very limited processing. We applied two steps: making the representation of the full field vector consistent in the data, and de-trending to remove the main field, secular variation and the influence of the local crust. This is philosophically different from other approaches often employed to study the magnetosphere-ionosphere system that usually perform operations such as rotation of the horizontal component into a magnetic north reference frame (e.g. Gjerloev 2012). We take the data set reported by each

station and compute the remaining missing components to give the full set: X, Y, Z, H, F, D, I . Although it is common for a separate F value to be reported (which comes from a proton precession magnetometer), we usually ignore it and compute F solely from the other components, unless only D, I, F are reported.

Magnetometers at observatories and variometer stations measure contributions to the geomagnetic field vector from Earth's core and the local lithosphere as well as the external field. As we wish to remove the internal sources, there

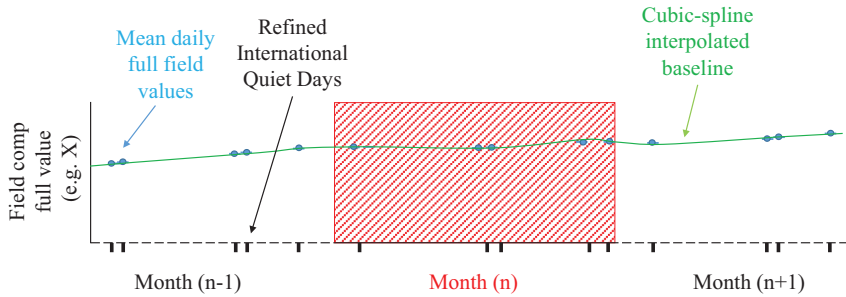


Figure 2 Schematic of the baseline construction scheme. For each component, the mean value of all minute-mean data on each of the five refined international quiet days per month are used to fit a cubic-spline curve. Data from the months prior to and after the current month are used to control the curve.

are a number of possible approaches for modelling the main field, secular variation and the fixed offset arising from local crustal fields, in order to isolate the external field component. The crustal offset is, in practice, not fully described by global modelling, so we turn to the data themselves for a method of extracting the external field contribution. There are various techniques and methods in the literature each of which bring their own advantages and drawbacks.

As an example, van de Kamp (2013) describes a method for estimating the background harmonic baseline to subtract from each station record. In his method, templates (or curves) are derived based on fitting a small number of sinusoidal harmonics to daily Sq curves from the quietest days in a given period. The long-term background is then removed by computing a linear interpolation between daily median values. Although this method has advantages in terms of consistency, it does remove the Sq variation in addition to the secular variation and crustal offset. In contrast, we wish to preserve as much of the external field signal within the data sets as possible, so use a different approach.

Instead, we wish to find the background quiet-time value for each observatory. From the list of international Quiet Days published by GFZ Helmholtz Centre, Potsdam, we use the quietest days per month according to the GFZ's 'refined' classification. A disadvantage of the usual classification of 'quiet' days is that during a highly active month there may be significant geomagnetic disturbances, even on the 'quietest' days. The use of the refined classification ameliorates this situation, rejecting days based on both relative and absolute activity levels, in which there are no values greater than Kp3 recorded. Hence, there may not always be designated quiet days if a month is particularly active.

We form the baseline for a given station over a month by computing the daily mean in each component over each of our quiet days, after which we use cubic spline interpolation to fill the gaps between quiet days. When de-trending a given time-series we use the refined quiet days and include a month's worth of data both before and after the period of

interest, in case it was an active month. This ensures we are correctly interpolating across the start and end of the month when finding the baseline to subtract. Figure 2 schematically illustrates the construction of the baseline. The external field values for each minute are given by:

$$B_{ext}^i = B_{full}^i - B_{baseline}^i \quad \forall i = X, Y, Z, H, F, D, I. \quad (1)$$

Finally we take a 14-day running mean over the resulting baseline values to smooth out any remaining variations caused by spline interpolation. We note this process effectively defines the external field by its frequency band, by filtering out long period components of the external field such as seasonal and annual variation. However, for this study we focus on the shorter period signals with frequencies below two weeks, though we acknowledge there are longer periods in the data.

Once this step has been completed for the seven components at all stations, the final stage is to compute the minute-by-minute comparison between each of the valid 267 station-pairs. These minute-mean differences for the overlapping years are then grouped and compared over a number of different time epochs depending on the length of the overlap of each pair, for example over the entire data set, or partitioned into hourly, monthly, annual, seasonal and solar-cycle phases.

2.3 Computing confidence intervals

Once the minute-mean differences are derived, the associated confidence intervals for each component are computed. As the probability distribution of differences in magnetic data tends towards being Laplacian rather than Gaussian (e.g. Walker and Jackson 2000), calculating the normal standard deviation (1σ) and multiplying by 2 or 3 is not the correct method for estimating the equivalent confidence intervals. Instead, the absolute (unsigned) differences are ordered by size and the values corresponding to the 68.3, 95.4 and 99.7 percentiles are recorded. This is repeated for all seven components for all data pairs in all combinations of time epochs. Note that we also computed the values for the signed pair differences, and

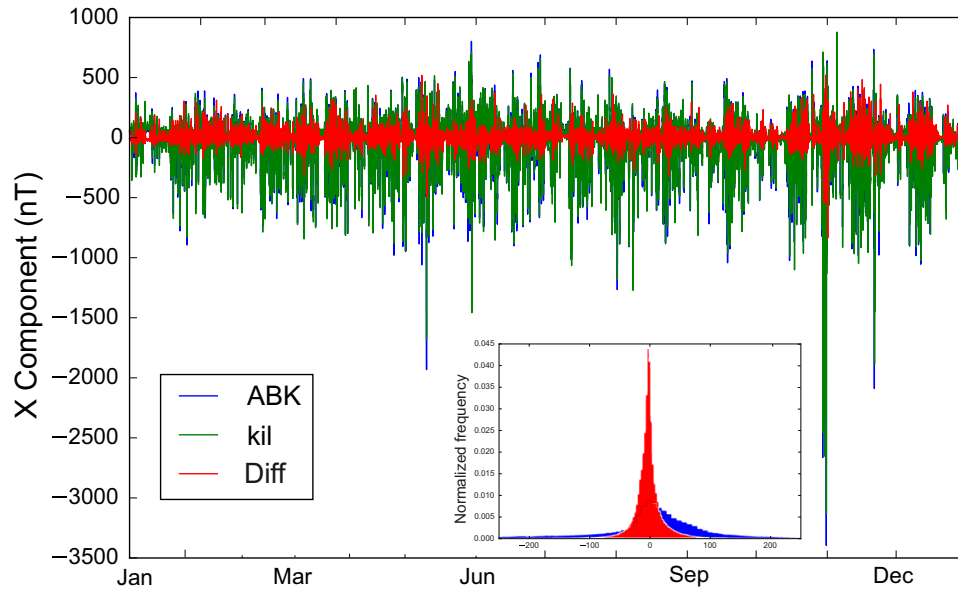


Figure 3 External fields in the north component (X) of the minute mean values from Abisko (ABK) and Kilpisjärvi (kil) and their differences for the year 2003. Inset shows the histogram of the external field of ABK and the differences between ABK and kil.

found they were very close to the unsigned pair differences (usually to within a few nT).

3 RESULTS

We computed the 68.3%, 95.4% and 99.7% confidence limits for all 267 station-pairs across a number of epochs including by hour, month, year, season (spring, summer, autumn, winter for the Northern hemisphere) and by solar cycle epoch (minimum, ascending, maximum, descending). When combined with the seven components of the field, this produces a large number of possible combinations when all components are considered, so we just concentrate on the seasonal and solar cycle temporal signals in the results as they illustrate the first order controls on the variation of the external field with respect to the strongest epoch influences. Before we discuss the aggregate statistical results, we will examine the differences between two sets of station-pairs: (1) Abisko and Kilpisjärvi in northern Scandinavia as a typical example; and (2) Deadhorse and Jim Carrigan Observatory in Alaska as a unique closely-spaced pair.

3.1 ABK and kil: a typical example

To illustrate the derivation of confidence intervals from external field data and the pair-wise differences, we examine Abisko (ABK) and Kilpisjärvi (kil), two stations separated by a

great circle distance of approximately 110 km, with Kilpisjärvi about one degree of latitude north of Abisko. Both lie between 65° and 66° N in quasi-dipole geomagnetic latitude. Figure 3 shows the de-trended data sets of the north (X) component for the year 2003 in which the external field values from each station strongly overlap, as expected. The differences between the minute-mean values are also plotted (red line), illustrating that the two stations experience approximately the same external field, though during active periods the differences grow much larger (e.g. 29–31 October 2003 storm).

Figure 3 also shows the normalized histogram (inset) of the external field values from Abisko and the differences between Abisko and Kilpisjärvi. The histogram of the external field values from Abisko has a pronounced positive skew, which suggests an eastward electrojet is more commonly observed at Abisko as the X component usually increases in strength during active periods rather than decreases (the histogram for Kilpisjärvi is very similar, not shown). The width of the differences between the stations is much narrower than the Abisko histogram, demonstrating that the two locations observe similar external magnetic field values.

The confidence intervals for the year 2003 of the X component at Abisko and Kilpisjärvi are given in Table 2. The distribution of the external field differences is clearly not Gaussian, as the computed 1σ standard deviation value is much larger than the equivalent confidence interval at 68.3%. For the differences between the two stations, the 1σ standard

Table 2 Table of 1σ standard deviation and 68.3%, 95.4% and 99.7% confidence intervals for the X component of Abisko (ABK), Kilpisjärvi (kil) and their unsigned differences for the year 2003 and over the period of a solar cycle (1995–2007)

X (nT)	1σ	2003			1σ	1995–2007		
		68.3%	95.4%	99.7%		68.3%	95.4%	99.7%
ABK	147.8	82.3	335.2	756.1	89.1	35.9	231.9	632.1
kil	147.3	87.9	331.0	740.1	90.0	41.9	239.0	626.2
Difference	26.1	12.2	59.0	162.8	17.2	10.3	44.0	122.3

deviation estimate (26.1 nT) will be overly pessimistic for the 68.3% equivalent value (12.2 nT in this case) but lower than the actual difference at the 2σ equivalent level (59.0 nT) and severely underestimates the 3σ equivalent value (162.8 nT).

Over a longer period of approximately one solar cycle for the station-pair, covering 12 years from 1995 to 2007, the 1σ standard deviation estimate is 17.2 nT, which is larger than the 68.3% CI value of 10.3 nT. The 95.4% CI is 44.0 nT while the 99.3% is 122.3 nT. The reason for the smaller values (compared to the year 2003) is that longer time-series includes many quieter years, while 2003 was a very geomagnetically active year.

3.2 DED and JCO: accounting for observatory differences

A special case exists for two INTERMAGNET observatories located in northern Alaska. For non-scientific reasons, the Deadhorse observatory (DED), run by the US Geological Survey, is located around 350 m from the British Geological Survey's Jim Carrigan Observatory (JCO), both within the auroral zone at a geomagnetic latitude of 70° N. The spatial proximity of these two high-quality magnetic observatories allows us to investigate the differences due to instrumental, processing methodology and observation biases. Both sit on relatively non-magnetic tundra, as the measured site difference (between the absolute pillar and proton precession magnetometer) at JCO is 5.7 nT.

The DED observatory became operational in 2010, giving three years of definitive data to analyse against JCO (at the time of this study), though due to occasional collection gaps only 18 months are used. The observatories should, in theory, have identical external field measurements with zero mean difference between the outputs, once the main field, secular variation and crustal offsets have been removed. The differences that remain are due to variations in the instrumentation, observer biases in baseline measurements and the processing methodologies employed by the two institutes who run the observatories.

Though there are small differences between the external field values (not shown), the 95.4% confidence interval from the 18 months of data is 5.5 nT in the north component, 5.8 nT in the east component and 1.9 nT in the downward component and are within the INTERMAGNET-recommended tolerances. These values give us an expected lower limit for the differences between observatories. Between other stations, particularly remote variometers, additional differences will arise, for example where relatively few or no absolute measurements are made to account for instrument drift, or where the true orientation of the vector instrument is not well-controlled over time.

We next assess the aggregated results from all the station-pairs, focussing on the seasonal and solar cycle variations that show the largest variation over time.

3.3 Seasonal variation

The external field varies in intensity and activity level over the course of the solar year, controlled principally by the relative orientation of the Earth to the Sun's magnetic field. Magnetic activity generally increases during the equinoxes and decreases through to the winter and summer solstices (Russell and McPherron 1973), though this is itself modulated by the solar cycle. We examined the 68.3% and 95.4% confidence intervals for each of the seasons, finding that the winter season gives the smallest CI values, while autumn and spring have the largest values. Northern hemisphere summer tends to be more active than winter but not as active as the equinoxes.

To illustrate this, in Fig. 4 we show the 95.4% confidence intervals for three-month periods capturing the northern hemisphere winter solstice (December, January and February: DJF) and the autumnal equinox (September, October and November: SON). The CI are plotted as a function of east-west and north-south distances between observatories (regardless of the station-pair mean latitude). The plots show the station-pairs out to a distance of 1000 km in both directions. A robust linear interpolation technique employing radial

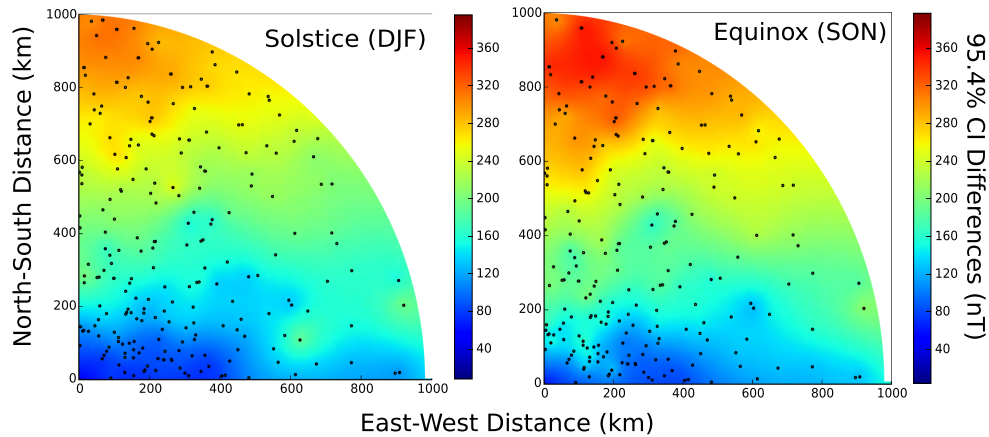


Figure 4 The 95.4% confidence intervals of the north component (X) for northern hemisphere winter solstice (DJF) (left column) and autumnal equinox (SON) (right column) as function of lateral distance. Station-pair locations are shown as closed circles.

basis functions (e.g. Torres and Barba 2009) has been used to smooth the data for the underlying colour map. The closed circles show the locations of the station-pairs forming the plots. Due to the geographical limitations of the available data, most of the station-pairs lie within 600 km, though around 20% of the pairs' separations exceed this distance. In this type of plot the variation of the magnitude of the CI with distance is clear. Along the east–west direction, the confidence limits increase more slowly than in the north–south direction. In the panels, there is a general north–south banded gradient, though with outliers attributable to the data quality. The 95.4% CI for the solstice are slightly lower than the equinox confirming that there is a modest increase in activity around the equinox periods.

3.4 Solar cycle variation

Over longer periods, the confidence intervals can be computed by grouping the time-series into specific phases of the solar cycle. For each paired time-series, we divided the data into minimum, ascending, maximum and descending phases based upon a retrospective analysis, which adjusts and normalizes the length of each phase period within each solar cycle. Using the smoothed (13-point running average) monthly mean A_p index from GFZ Potsdam (e.g. Rostoker 1972), the months with the minimum and maximum values are identified for each cycle and the total number of months per cycle are counted from minimum to minimum. We then allocate 25% of the total number of months to each of the minimum and maximum phases ensuring symmetry around the previously identified extrema. The remaining months in between are then allocated by default to either descending or ascending phases.

Figure 5 shows the CI limits plotted against north–south and east–west distance. In this plot the variation between minimum and maximum is clear. The minimum phase of the solar cycle has a lower overall magnitude compared to the maximum phase. The 95.4% CI plot for the solar maximum (right) has clear latitudinal gradient; that is, as the distance becomes larger in the north–south direction the colouring is strongly banded: the CI in the east–west direction vary around 125 nT over distances of 500 km, while the CI for stations separated by similar distance in the north–south direction, the CI rises to greater than 250 nT. Note as not all station-pairs span a full solar cycle, there are an unequal number of points in each phase. For clarity we show the results of the North component for two phases of the solar cycle, the minimum and maximum, which are chosen to illustrate the range of variability of the CI.

Comparing Figs. 4 and 5 suggests that the average magnitude of the seasonal variation is larger than the solar minimum though smaller than the maximum. Although not directly comparable, as the solar cycle encompasses several years of data, the plots show the complexity of the variation. We point out that although we have focused on the north (X) component for our results presented here, similar patterns are present in all other components of the magnetic field. Further plots for each component, including for the 68.3% and the 99.7% CI, are available in the supplementary material.

3.5 Overall CI plots

To investigate the CI in more detail, slices or transects along the east–west and north–south directions were taken from the plots shown in the panels of Figs. 4 and 5. These transects

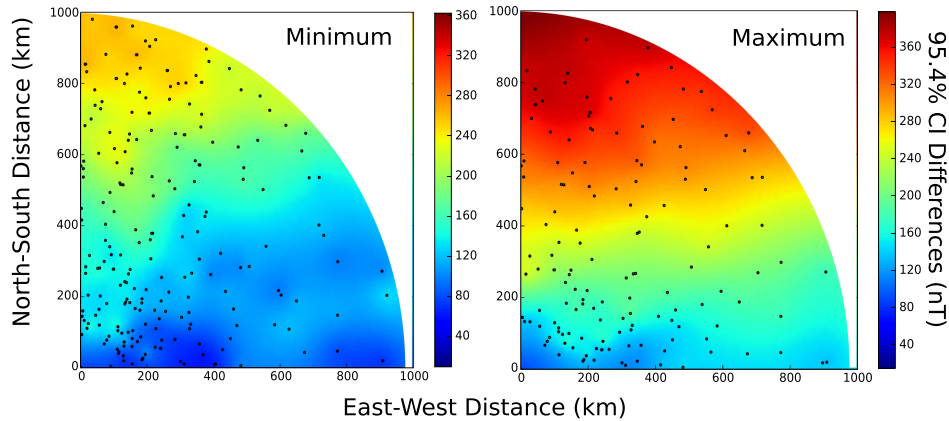


Figure 5 The 95.4% confidence intervals of the north component (X) for the minimum (left column) and maximum (right column) phases of the solar cycle as a function of lateral distance. Station-pairs are shown as closed circles.

show the variation with distance from the origin. An east–west transect through each interpolated data set passes along the lower edge of each panel of Figs. 4 and 5 (i.e. zero north–south distance) while a north–south line is a slice through the left-hand edge (i.e. zero east–west distance) of these panels.

Figure 6 shows the transects through the interpolated CI versus distance of all seven magnetic components (X , Y , Z , H , F , declination and inclination). The upper panel of Fig. 6 is the X component derived from the interpolated data shown in Figs. 4 and 5. The solid lines represent the 68.3% CI (which are not shown) while the dashed lines are the 95.4% CI (as shown). For completeness, a 45° transect from the origin towards the upper-right corner of each panel is also plotted. We also show the plots using all available data from all times (ALL).

It is clear that the lines are not close to the origin at zero distance between the station-pairs. In the X component, the minimum 68.3% CI at the origin is around 11 nT for the solar cycle minimum while for the maximum phase of the cycle the 68.3% CI is 35 nT. We do not expect the remnant crustal field to have much influence as our baseline removal technique is designed to exclude this source, so this implies there are other reasons for the differences.

In Fig. 6, the gradients of the east–west lines are typically low, around 25–75 nT/1000 km in many plots for both 68.3% CI for the seasonal (DJF, SON) and solar minimum epochs. The relatively flat gradients in this direction imply that an observer at some distance from a station at the same geomagnetic latitude can usefully apply the measurements at a remote location. The gradients of the north–south lines are larger, ranging from around 70 nT/1000 km and 250 nT/1000 km for solar minimum 68.3% and 95.4% CI,

respectively. For the solar maximum, the north–south gradients are largest; from around 125 nT/1000 km and > 400 nT/1000 km for the 68.3% and 95.4% CIs, respectively. The values for all data available (ALL) are actually slightly lower than those for the solar maximum.

Note, the X component has the largest variation of all components which is why we focus mainly on it. Inspection of the supplementary materials shows similar behaviour in the other components across the seasonal and solar cycle phases. Table 3 provides the coefficients for the linear slope and offset from zero derived from straight-lines fits through data from all times for the east–west and north–south transects from the ALL panels of Fig. 6.

4 DISCUSSION

We emphasize again that the variations reported are related to spatial changes between sites and represent the time-average differences over the noted periods (i.e. seasonal, solar cycle phase). They should not be confused with actual variation experienced at high latitudes, especially during geomagnetic storms. The results presented show phenomena already well understood, i.e. the ability to predict geomagnetic external field values reduces with increasing distance at high latitudes, particularly in the north–south direction (e.g. Chapman and Bartels 1940, Chapter 9). However, they do provide some new insights as there are no published results on the analysis of confidence intervals at high geomagnetic latitudes over long temporal periods, from seasonal to solar cycle variations. This analysis examines the variation with direction (east–west and north–south) rather than as a single average value describing

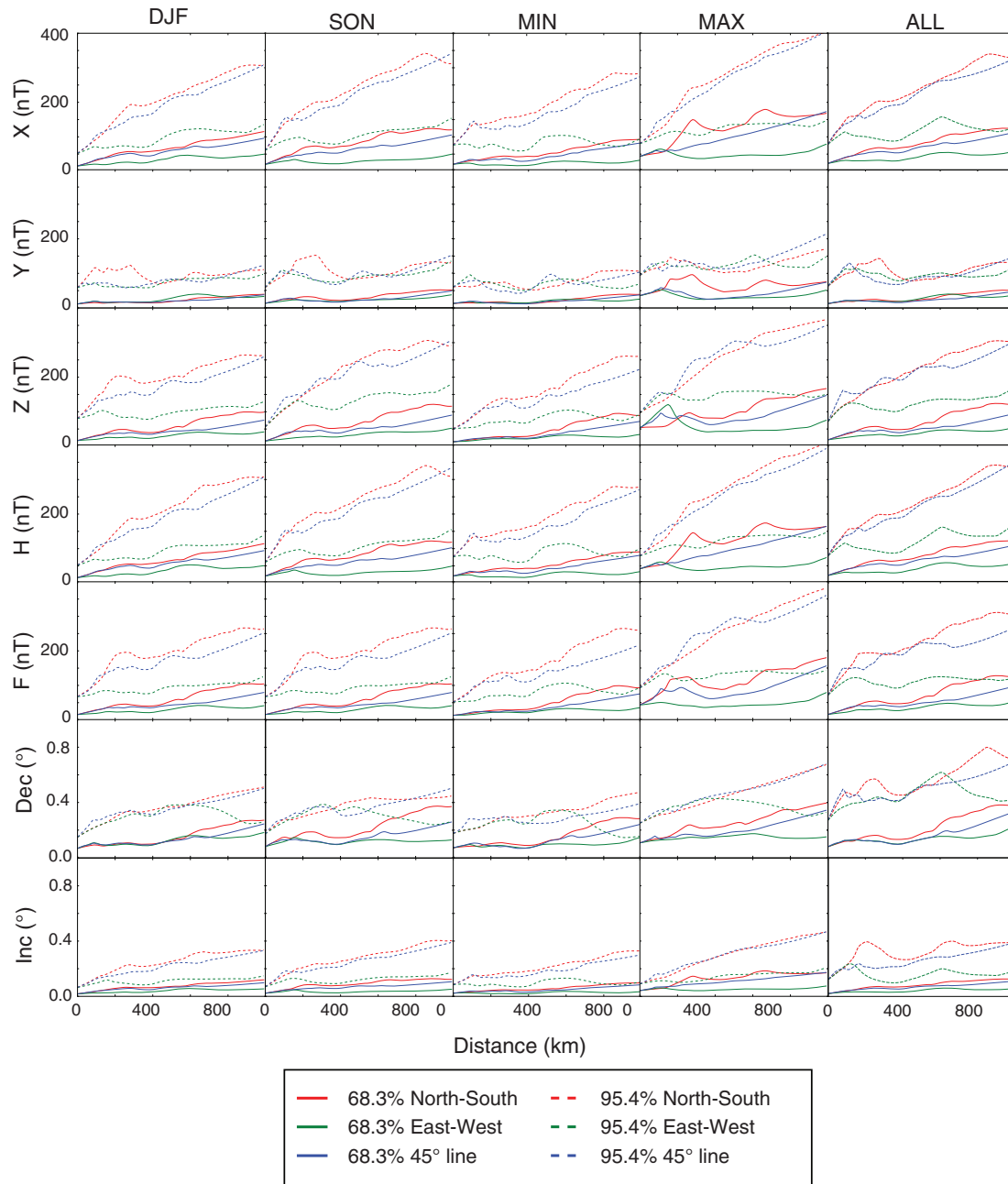


Figure 6 Transects from the interpolated CI differences of all components between station-pairs for the winter solstice (DJF), autumnal equinox (SON), the solar cycle minimum (MIN) and maximum (MAX) phases and for all available data (ALL). See text for details.

the data set without temporal or spatial context. This is far more useful for applying the results in a pragmatic sense.

4.1 Non-zero offset

An unexpected result is the ubiquitous offset of all the curves from the origin in Fig. 6. This may be attributed

to one or more of the following effects: (1) time-varying magnetic induction or geoelectric fields generated by magnetic fields and local geological features, (2) the use of all station-pair distances regardless of geomagnetic latitude, (3) differences in instrumentation and data processing protocols between sites and (4) the smoothing applied by the radial basis interpolation.

Table 3 Table of the linear (*a*) and offset (*b*) coefficients of the first-order polynomial fit (i.e. $y = ax + b$) for all available data (from the ALL panels in Fig. 6)

Component (Linear; Offset)	All Time CI 68.3%	All Time CI 95.4%
X (nT/km, nT)		
EW	(0.033, 18.7)	(0.131, 74.9)
NS	(0.104, 18.7)	(0.317, 74.9)
Y (nT/km, nT)		
EW	(0.023, 12.8)	(0.034, 63.6)
NS	(0.039, 12.8)	(0.072, 63.6)
Z (nT/km, nT)		
EW	(0.034, 15.2)	(0.108, 68.4)
NS	(0.104, 15.2)	(0.309, 68.4)
H (nT/km, nT)		
EW	(0.034, 18.5)	(0.137, 76.1)
NS	(0.102, 18.54)	(0.306, 76.1)
F (nT/km, nT)		
EW	(0.035, 15.1)	(0.088, 71.1)
NS	(0.110, 15.1)	(0.304, 71.1)
D (deg/km; deg)		
EW	(1.41e-04, 0.08)	(3.652e-04, 0.270)
NS	(3.04e-04, 0.08)	(5.371e-04, 0.270)
I (deg/km; deg)		
EW	(3.46e-05, 0.02)	(6.93e-05, 0.12)
NS	(1.06e-04, 0.02)	(3.70e-04, 0.12)

The largest part of the variation is most likely attributable to the effects of magnetic induction from the local geology at each station. Even relatively close stations can show differences as lithological conductivity can vary widely over short distances, for example in highly magnetised regions around igneous rocks (Ingham and Hutton 1982). Other possible reasons for local variation have been attributed to the induction effects of soils or long-term dissipation of magnetization from lightning strikes (e.g. Shimizu *et al.* 2007; Mishima *et al.* 2013).

The next largest effect is from the difference in latitude between station-pairs. Investigation of this effect (not shown) suggests that stations-pairs at very high latitude (over 70°) have larger differences than pairs at low latitude. Hence, some of the points that are relatively close in great-circle distance (and near the origin in these plots) but at high latitudes will contribute to the offset. However, most of the station-pairs lie between 60° and 66°.

Many of the stations used are variometers that usually have a lighter calibration and baseline measurement regime than observatories. As shown in Section 3.2, the instrumentation and processing protocols of DED and JCO can explain

around 5 nT of the offset, though for other stations this may be larger. This implies that the source of the offset is within the data itself, rather than from the smoothing technique used.

To construct the plots in Figs. 4 and 5, we used station-pairs from all geomagnetic latitudes, juxtaposing stations from both auroral and peri-auroral regions that may produce outliers. Due to the smoothing from the radial basis functions, large discrepancies will be visible as ‘islands’ in the plots and while there are a few outliers, none are close to the origin. Experimentation with the smoothing parameter for the interpolation showed that even very strong smoothing produced an offset at the origin.

Other possible effects are large steps or spikes in the data that were not detected in the quality-control stage, though these should be smoothed out by the interpolation and filtering. We present the plots as derived to show the effect that spatial density, coverage and overall data quality have on the solutions.

From Figs. 4 and 5 it is clear that the average equinox variation is larger than the variation during the solar minimum. Indeed, the solar maximum CI values are not much larger than the equinox variation either. This suggests that the seasonal variation is almost equivalent, on average, to that of the solar cycle variation for the years included in the study. From this observation, we conclude that one should pick the seasonal variation as more conservative estimate of the CI during solar minimum, otherwise choose the solar maximum values. The values for data from all times fall below those of solar maximum so are more optimistic. We note the non-zero differences between two stations, even at close range such as DED and JCO, suggests that in reality there will always be a non-zero error in any external field extrapolation.

4.2 Applications

As an example of how to apply the results in Fig. 6 and Table 3, we outline a few possible scenarios. We first consider an aeromagnetic survey at high geomagnetic latitudes over a large expanse of water. This situation occurs in the Arctic Ocean where the lithospheric field is the target of interest (e.g. Vogt *et al.* 1979). A total magnetic field (*F*) survey typically uses a single base station on land to monitor diurnal variation or remove the external field influence, with further post-processing usually required to align the measured data together. Such surveys are acquired in summer, ideally during low geomagnetic conditions (Watermann, Gleisner and Rasmussen 2011). However, there will still be external field activity at high latitudes. During a survey, the

F component CI suggests a survey can extend over 425 km from the station in an east–west direction and remain within 30 nT of the measured external field values at the base-station up to 68.3% of the time (i.e. $\frac{30-15.1}{0.035}$). For the north–south direction, the value at 425 km northward is approximately 60 nT (i.e. $425 * 0.102 + 15.1$). At the 95.4% interval, the east–west direction suggests an uncertainty of around 110 nT at 425 km, while the north–south value is 200 nT. Although the true value is strongly controlled by local activity at the time of the measurement flights, the CI provides an envelope for the uncertainty at the planning stages. For post-processing of the data, a gross threshold can be placed on the magnitude of tie-line intersection errors ahead of time, allowing a quick rule-of-thumb to be established based on expected variability of the magnetic field in general, or at a particular part of the year or solar cycle.

Other applications include the use of the confidence intervals in directional drilling in order to control the down-hole error ellipses while undertaking wellbore steering towards a specific underground target. For our second case, we estimate the error on the declination, inclination and total field components with distance from the observatory location. These can be used to assess the level of uncertainty at the drilling location and help avoid missing the intended target or intersecting with another well. Consider an offshore well being drilled at high-latitude at a distance of 400 km in an easterly direction from an observatory. From Table 3, the 68.3% CI for the difference in declination would be $D = 400 * 0.000141 + 0.08 = 0.136^\circ$, the inclination difference would be $I = 400 * 0.0000346 + 0.02 = 0.033^\circ$ and the total field would be $F = 400 * 0.035 + 15.1 = 29.1$ nT. For a drill site in a northerly direction from an observatory, the uncertainty values can be computed in a similar manner.

5 CONCLUSIONS

We address the question of how far away from an observatory at high latitude can external magnetic field data be usefully extrapolated. Though a seemingly simple question to ask, the answer relies on a large number of time-varying parameters. Many studies have shown that external field extrapolation with two or more stations improves the accuracy of the result compared to just a single station. Therefore, the confidence intervals computed are for the worst-case scenario where only one station is used to predict the field at another location. However, this case is usually the most common and thus it is important to know how far away from a station the external magnetic field be reasonably applied.

We examined the minute-mean differences from over 3000 years of station-pairs at high geomagnetic latitude ($58^\circ < |\theta_{gm}| < 75^\circ$) and used them to compute confidence intervals for the 68.3, 95.4 and 99.7 percentiles. From these confidence intervals, the general errors involved in using data from a single observatory or variometer to infer the external magnetic field values at distances of up to 1000 km can be estimated. We examined the variation in confidence limits over distances of up to 1000 km in both the east–west and north–south directions, and investigated the changes over solar cycle phases and seasonal periods and all of the data. We provide coefficients for simple linear fits to the differences in the north–south and east–west direction.

We find that there is always a small bias away from zero difference even at closely-spaced observatories. Using station-pair differences from all available data we find the bias is between 10–20 nT depending on the component. In the X component of the external field, the east–west confidence intervals have relatively low variation at around 11 nT/1000 km during the less active periods of the year and solar minimum conditions for the 68.3% CI. Gradients in the north–south directions for the X component are larger at around 71 nT/1000 km for 68.3% CI during solar minimum. For the solar maximum and equinox periods, the gradients become larger.

For more active periods, the variation obviously becomes larger. However, it is presently unclear which activity index is best to compare the errors to, though obvious candidates are K , K_p , A_p or AE . Further work will be carried out to resolve this question.

ACKNOWLEDGEMENTS

We thank the institutes who make magnetic field measurements and help maintain the worldwide network. We thank the national institutes that support them and INTERMAGNET for promoting high standards of magnetic observatory practice. We acknowledge the World Data Centre for Geomagnetism, Edinburgh and we thank the institutes that maintain the IMAGE Magnetometer Array. All data were obtained, analysed, and visualized using open source software tools in scientific Python, in particular we acknowledge the developers of the ‘requests’, ‘NumPy’, ‘pandas’ and ‘matplotlib’ libraries (Hunter 2007; van der Walt, Colbert and Varoquaux 2011; McKinney 2012). Refined quiet day and A_p values are available from the GeoForschungZentrum, Potsdam. We thank the two anonymous reviewers for their constructive comments on the initial drafts of this manuscript. This paper is published

with the permission of the Executive Director of the British Geological Survey (NERC).

ORCID

Ciarán D. Beggan  <http://orcid.org/0000-0002-2298-0578>

REFERENCES

- Amm O. and Viljanen A. 1999. Ionospheric disturbance magnetic field continuation from the ground to the ionosphere using spherical elementary current systems. *Earth Planets Space* **51**, 431–440.
- Campbell W. 2003. *Introduction to Geomagnetic Fields*. Cambridge, UK: Cambridge University Press.
- Chapman S. and Bartels J. 1940. *Geomagnetism*. Clarendon Press.
- Constable C. 2015. Earth's electromagnetic environment. *Surveys in Geophysics* **37**, 27–45.
- Dawson E., Nkisi-Orji I., Reay S. and Macmillan S. 2013. Geomagnetism data portal: a new service from the World Data Centre, Edinburgh. In: *IAGA 12th Scientific Assembly*. British Geological Survey. <http://nora.nerc.ac.uk/503053/>.
- Dods J., Chapman S.C. and Gjerloev J.W. 2015. Network analysis of geomagnetic substorms using the SuperMAG database of ground-based magnetometer stations. *Journal of Geophysical Research: Space Physics* **120**, 7774–7784.
- Edwardsen I., Johnsen M.G. and Lovhaug U.P. 2016. Effects of substorm electrojet on declination along concurrent geomagnetic latitudes in the northern auroral zone. *Journal of Space Weather and Space Climate* **6**, 1–16.
- Emmert J.T., Richmond A.D. and Drob D.P. 2010. A computationally compact representation of magnetic-apex and quasi-dipole coordinates with smooth base vectors. *Journal of Geophysical Research: Space Physics* **115**.
- Finlay C.C., Maus S., Beggan D.C., Hamoudi M., Lowes J.F., Olsen N. *et al.* 2010. Evaluation of candidate geomagnetic field models for IGRF-11. *Earth, Planets and Space*, **62**, 787–804.
- Gaunt C. 2016. Why space weather is relevant to electrical power systems. *Space Weather* **14**, 2–9.
- Gjerloev J.W. 2012. The SuperMAG data processing technique. *Journal of Geophysical Research: Space Physics* **117**, A09213.
- Gjerloev J.W. and Hoffman R.A. 2014. The large-scale current system during auroral substorms. *Journal of Geophysical Research: Space Physics* **119**, 4591–4606.
- Gleisner H., Rasmussen O. and Watermann J. 2006. Large-magnitude geomagnetic disturbances in the North Sea region: statistics, causes, and forecasting. *Advances in Space Research* **37**, 1169–1174.
- Hunter J.D. 2007. Matplotlib: A 2D graphics environment. *Computing in Science & Engineering* **9**, 90–95.
- Ingham M.R. and Hutton V.R.S. 1982. Crustal and upper mantle electrical conductivity structure in Southern Scotland. *Geophysical Journal International* **69**, 579–594. <http://gji.oxfordjournals.org/content/69/3/579.abstract>.
- Juusola L., Kauristie K., van de Kamp M., Tanskanen E.I., Mursula K., Asikainen T., *et al.* 2015. Solar wind control of ionospheric equivalent currents and their time derivatives. *Journal of Geophysical Research: Space Physics* **120**, 4971–4992.
- van de Kamp M. 2013. Harmonic quiet-day curves as magnetometer baselines for ionospheric current analyses. *Geoscientific Instrumentation, Methods and Data Systems* **2**, 289–304.
- McHenry M. and Clauer C. 1987. Modeled ground magnetic signatures of flux transfer events. *Journal of Geophysical Research* **92**, 11231–11240.
- McKinney W. 2012. *Python for Data Analysis: Data Wrangling with Pandas, NumPy, and IPython*. California, USA: O'Reilly Media.
- McLay S. and Beggan C. 2010. Interpolation of externally-caused magnetic fields over large sparse arrays using Spherical Elementary Current Systems. *Annales Geophysicae* **28**, 1795–1805.
- Mishima T., Owada T., Moriyama T., Ishida N., Takahashi K., Nagamachi S., *et al.* 2013. Relevance of magnetic properties of soil in the magnetic observatories to geomagnetic observation. *Earth, Planets and Space* **65**, 337–342.
- Olsen N., Hulot G., Lesur V., Finlay C.C., Beggan C., Chulliat A., *et al.* 2015. The Swarm initial field model for the 2014 geomagnetic field. *Geophysical Research Letters* **42**, 1092–1098.
- Reay S.J., Allen W., Baillie O., Bowe J., Clarke E., Lesur V. *et al.* 2005. Space weather effects on drilling accuracy in the North Sea. *Annales Geophysicae* **23**, 3081–3088.
- Reeves C. 1993. Limitations imposed by geomagnetic variations on high quality aeromagnetic surveys. *Exploration Geophysics* **24**, 115–116.
- Ritter P. and Lühr H. 2008. Near-Earth magnetic signature of magnetospheric substorms and an improved substorm current model. *Annales Geophysicae* **26**, 2781–2793.
- Rostoker G. 1972. Geomagnetic indices. *Reviews of Geophysics* **10**, 935–950.
- Russell C. and McPherron R. 1973. Semiannual variation of geomagnetic activity. *Journal of Geophysical Research* **78**, 92–108.
- Sabaka T.J., Olsen N., Tyler R.H. and Kuvshinov A. 2015. CM5, a pre-Swarm comprehensive geomagnetic field model derived from over 12 yr of CHAMP, Ørsted, SAC-C and observatory data. *Geophysical Journal International* **200**, 1596–1626.
- Shimizu H., Koyama T., Koyama S. and Utada H. 2007. A geomagnetic total intensity anomaly originated from lightning-induced isothermal remanent magnetization: case of the Yatsugatake Magnetic Observatory, central Japan. *Earth, Planets and Space* **59**, 141–149.
- Tanskanen E.I. 2009. A comprehensive high-throughput analysis of substorms observed by IMAGE magnetometer network: Years 1993–2003 examined. *Journal of Geophysical Research: Space Physics* **114**.
- Thébault E., Purucker M., Whaler K.A., Langlais B. and Sabaka T.J. 2010. The magnetic field of the Earth's lithosphere. *Space Science Reviews* **155**, 95–127.
- Torres C.E. and Barba L. 2009. Fast radial basis function interpolation with Gaussians by localization and iteration. *Journal of Computational Physics* **228**, 4976–4999.
- Vogt P.R., Taylor P.T., Kovacs L.C. and Johnson G.L. 1979. Detailed aeromagnetic investigation of the Arctic basin. *Journal of Geophysical Research: Solid Earth* **84**, 1071–1089.

- Walker M.R. and Jackson A. 2000. Robust modelling of the Earth's magnetic field. *Geophysical Journal International* **143**, 799–808.
- van der Walt S., Colbert C.S. and Varoquaux G. 2011. The numpy array: a structure for efficient numerical computation. *Computing in Science & Engineering* **13**, 22–30.
- Watermann J., Gleisner H. and Rasmussen T. 2011. A geomagnetic activity forecast for improving the efficiency of aeromagnetic surveys in Greenland. *Advances in Space Research* **47**, 2172–2181.
- Watermann J., Rasmussen O., Stauning P. and Gleisner H. 2006. Temporal versus spatial geomagnetic variations along the west coast of Greenland. *Advances in Space Research* **37**, 1163–1168.
- Waters C.L., Gjerloev J.W., Dupont M. and Barnes R.J. 2015. Global maps of ground magnetometer data. *Journal of Geophysical Research: Space Physics* **120**, 9651–9660.